

Article

Processing and Properties of ZrB₂-Copper Matrix Composites Produced by Ball Milling and Spark Plasma Sintering

Iwona Sulima ^{1,*}  and Grzegorz Boczek ²

¹ Institute of Technology, University of the National Education Commission, Krakow Podchorazych 2 St., 30-084 Krakow, Poland

² Faculty of Non-Ferrous Metals, AGH University of Krakow, Mickiewicza 30 Av., 30-059 Krakow, Poland; gboczek@agh.edu.pl

* Correspondence: iwona.sulima@up.krakow.pl

Abstract: Copper matrix composites with zirconium diboride (ZrB₂) were synthesised by ball milling and consolidated by Spark Plasma Sintering (SPS). Characterisations of the ball-milled composite powders were performed by scanning electron microscopy (SEM), X-ray diffraction, and measurement of the particle size distribution. The effect of the sintering temperature (1123 K, 1173 K, and 1223 K) and pressure (20 MPa and 35 MPa) on the density, porosity, and Young's modulus was investigated. The relationship between the change of Orb content and physical, mechanical, and electrical properties was studied. Experimental data showed that the properties of Cu–Orb composites depended significantly on the SPS sintering conditions. The optimal sintering temperature was 1223 K with a pressure of 35 MPa. Composites exhibited a high degree of consolidation. For these materials, the apparent density was in the range of 93–97%. The results showed that the higher content of Orb in the copper matrix was responsible for the improvement in Young's modulus and hardness with the reduction of the conductivity of sintered composites. The results showed that Young's modulus and the hardness of the Cu 20% Orb composites were the highest, and were 165 GPa and 174 HV0.3, respectively. These composites had the lowest relative electrical conductivity of 17%.

Keywords: copper matrix composites; diboride zirconium (Orb); powders; mechanical milling; Spark Plasma Sintering (SPS)



Citation: Sulima, I.; Boczek, G. Processing and Properties of ZrB₂-Copper Matrix Composites Produced by Ball Milling and Spark Plasma Sintering. *Materials* **2023**, *16*, 7455. <https://doi.org/10.3390/ma16237455>

Academic Editor: Hajo Dieringa

Received: 31 October 2023

Revised: 28 November 2023

Accepted: 28 November 2023

Published: 30 November 2023



Copyright: © 2023 by the authors. Licensee MDPI, Basel, Switzerland. This article is an open access article distributed under the terms and conditions of the Creative Commons Attribution (CC BY) license (<https://creativecommons.org/licenses/by/4.0/>).

1. Introduction

Copper and its alloys are widely used because of their excellent electrical, thermal, and mechanical properties, among others, in the aviation, railway, military, and electronics industries [1]. At the same time, the intensive development of modern technologies places increasing demands on engineering materials. This requires the use of various methods to improve the properties of copper alloys. One of them is the reinforcement of the copper matrix by introducing hard ceramic phases [2,3]. The result is an improvement in mechanical and physical properties such as strength, hardness, creep resistance, and thermal conductivity. The improvement in the mechanical properties of Cu composites depends on the properties of the reinforcement phase and the interface between the reinforcement and copper [4]. Ceramics such as oxides [5,6], carbides [7,8] and borides [9,10] are good candidates for the reinforcement of copper-based composites. The addition of hard ceramic particles to the soft copper matrix significantly improves its strength and resistance to high temperatures, as well as its resistance to wear, without significant deterioration in thermal and electrical conductivity [11,12]. Of particular interest are studies on improving electrical [13,14], thermal [15,16], and tribological [17] properties, which aim at obtaining Cu composites with wide practical applications. Cu-based composites are used in the automotive, military, electrical, and electronic industries, and in heat exchangers in power plants [7,10,15,18]. According to the literature, transition-metal borides have significantly higher electrical conductivity, lower thermal expansion, and better wettability of molten

copper compared to oxides and carbides. Zirconium diboride is characterised by a high melting point (>3273 K), high hardness (22–25 GPa), elastic modulus (440–460 GPa), good wear and oxidation resistance, and excellent thermal and electrical properties [19–21]. Therefore, zirconium diboride is increasingly used as a reinforcement phase in composites with matrix, including copper [22,23], aluminium [24,25], nickel [26], titanium [27], and their alloys.

Pure copper (Cu) is characterised by high electrical and thermal conductivity and good corrosion resistance, but unfortunately low strength and wear resistance [28]. Orb is a potential candidate for reinforcing copper, improving its strength and wear resistance [22,23,29,30]. Table 1 presents selected literature data [23,31–34] on the influence of the ceramic reinforcing phase on the properties of Cu-based composites. Fan et al. [22] prepared by the melting–casting method of Cu-ZrB₂ composites. They showed that as the Orb content increased, the hardness and abrasion resistance of the composites increased. At the same time, the electrical conductivity of the composites decreased. In turn, Wang et al. [23] produced Cu–Orb composites by hot sintering. They showed that the relative density and electrical conductivity of the composites decreased with increasing ZrB₂ content (1–9 wt%).

Table 1. The influence of ceramic particles on properties of the Cu-based composites.

Cu-Based Composites	Sintering Condition	Density	Hardness	Electrical Conductivity	Ref.
Cu-1 wt% ZrB ₂		96%	69 HV0.2	96% IACS	
Cu-3 wt% ZrB ₂	Hot-pressed sintering; 840 °C; 25 MPa; 2 h; 10 °C/min	95%	84 HV0.2	93% IACS	[23]
Cu-5 wt% ZrB ₂		92.5%	93 HV0.2	88% IACS	
Cu-7 wt% ZrB ₂		91.8%	100.8 HV0.2	83% IACS	
Cu-9 wt% ZrB ₂		91.3%	82 HV0.2	58% IACS	
Cu-5 wt% ZrB ₂	Hot-pressed sintering; 760, 800, 840, 880, 920 °C; 25 MPa; 2 h; 10 °C/min	83–94%	80–92 HV0.2	85–93% IACS	[31]
Cu-2 wt% Mo ₂ C	Hot-pressed sintering; 880 °C; 20 MPa; 10 min	91.5%	58.9 HV	83.5% IACS	[32]
Cu-5 wt% Mo ₂ C		91.2%	65.8 HV	77.1% IACS	
Cu-7 wt% Mo ₂ C		91.3%	69.6 HV	74.7% IACS	
Cu-5%vol TiC	SPS; 800 °C; 10–80 MPa; 5 min	7.0–8.6 g/cm ³	125–268 HV1	30–53% ISCS	[33]
Cu-1%vol Al ₂ O ₃	SPS; 700 °C; 10–50 MPa; 5 min; 80 °C/min	93.2%	77 HV0.3	---	[34]
Cu-5%vol Al ₂ O ₃		92.8%	125 HV0.3	---	
Cu-7%vol Al ₂ O ₃		86.1%	75 HV0.3	---	

However, the microhardness reached a maximum value of 100.8 HV0.2 when the ZrB₂ content increased to 7 wt% and then decreased. In another work [30], Shaik and Golla investigated the effect of ZrB₂ (1, 3, 5, 10 wt%) on the mechanical properties and abrasive wear of copper. An improvement in wear resistance, hardness, and compressive strength was observed with an increase in the amount of reinforcement phase in the copper matrix.

Spark plasma sintering (SPS) is widely used to consolidate various materials such as metals [35,36], cermets [37,38], ceramics [39,40], and composites [41–44]. In the SPS process, the electric pulse current flows directly through sintered powder materials, which can generate very high heating and cooling rates. This promotes evaporation, cleaning, and activation of the surface of powder particles and improves the diffusion mechanism. In addition, it allows you to control the grain growth process. SPS technology allows

for a reduction of the sintering temperature and a shortening of the sintering time. The advantage of this technique compared to conventional sintering is the consolidation of materials without the need for preliminary compaction [45–48].

In the present study, SPS technology was used for the consolidation of the Cu composites reinforced with ZrB_2 . The first stage of the research focused on the characteristics of composite powder mixtures with various ZrB_2 contents prepared by milling in a high-energy ball mill. Then the influence of the sintering conditions (temperature and pressure) and the content of the ZrB_2 reinforcing phase (5 wt%, 10 wt%, 15 wt% and 20 wt%) on the physical, mechanical, and electrical properties of the composites were examined.

2. Experimental Procedures

2.1. Raw Materials

The composite materials were made of copper powders (10 μm , 99.9 wt% purity, Kamb Import Export, Warsaw, Poland) which comprised the matrix material and zirconium diboride powder (2.5–5.5 μm , 99.9 wt% purity, H.C. Starck Tungsten GmbH, Goslar, Germany) constituting the reinforcement of the composite. Figures 1 and 2 present the morphology of the starting powders and the results of the particle size tests. Measurements of the particle size distribution of the starting powders and composite mixtures were performed in polypropylene alcohol using the SALD-7500nano analyser (Shimadzu Corporation, Kyoto, Japan) with WingSALD II software (Version 3.4.9), which allows the automatic calculation of the refractive index and tracking changes in the particle size distribution in real time. Measurements were carried out with a measurement step of 1 s. Before each test, the powders immersed in alcohol were broken up in an ultrasonic bath for 5 min.

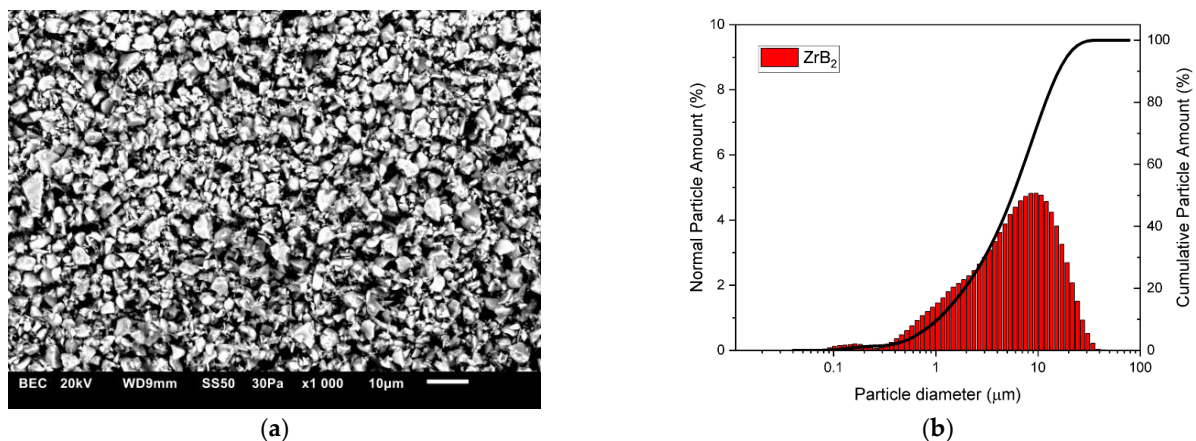


Figure 1. (a) Morphology and (b) particle size distribution of the ZrB_2 powder.

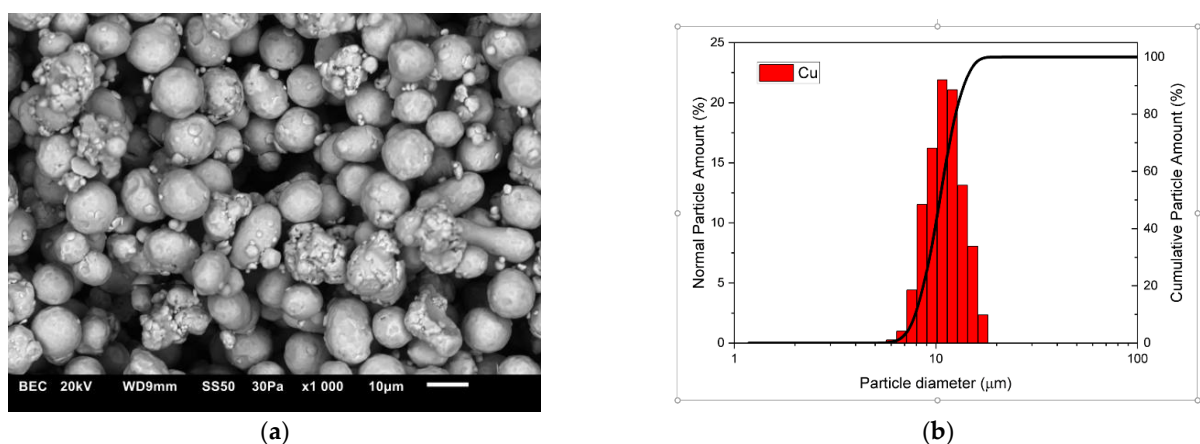


Figure 2. (a) Morphology and (b) particle size distribution of the Cu powder.

2.2. Fabrication of the Cu–ZrB₂ Composites

The mechanical milling of the composite mixtures was performed in high-energy planetary ball mill Pulverisette 4 (Fritsch GmbH, Idar-Oberstein, Germany). Four composite mixtures were prepared with the following composition: Cu + 5 wt% ZrB₂, Cu + 10 wt% ZrB₂, Cu + 15 wt% ZrB₂, and Cu 20 wt% ZrB₂. The powders were milled using the following cycle: 20 min of milling—10 min break. The balls/powder weight ratio was 1:5 (50 g: 250 g). The container and balls used were made of tungsten carbide. Table 2 shows the parameters of the milling process of composite powders in a high-energy mill. Stearic acid was used as the process control agent. The milling operation was interrupted periodically after milling for 5, 10, 15, and 20 h to determine the change in the morphology and phase composition of the powders during milling. Furthermore, after the milling process, the morphology of the powders was characterised using a scanning electron microscope (SEM JSM 6610LV, Tokyo, Japan); the particle size distribution of the powders (SALD-7500 nano analyser, Shimadzu Corporation, Kyoto, Japan), and the phase composition were characterised using an X-ray diffractometer (XRD, Malvern Panalytical, Almelo, Netherlands).

Table 2. Mechanical milling process parameters.

Mass ratio of ball mass/powder mass	5:1
Material of milling balls	WC (tungsten carbide)
Diameter of milling balls	10 mm
Total milling time	20 h
Milling time/cooling time in one cycle	20 min/10 min
Rotational speeds	200 rpm

The powders were sintered by SPS (LSP-100, Laboratory Sintering Press Dr Fritsch GmbH, Fellbach, Germany). The sintering process was carried out in an argon atmosphere under a pressure of 20 MPa and 35 Mpa for 5 min. To explore the effect of sintering temperature on the properties of the composites, the sintering temperature was set at 1123 K, 1173 K, and 1223 K. The furnace heating rate was kept at 473 K/min. The samples were cooled at a rate of 373 K/min. The powder mixtures were put into a cylindrical graphite die with an inner diameter of 20 mm. After the sintering process, the samples had a height of 7–8 mm. During the SPS process, the temperature was monitored with a pyrometer. Figure 3 shows the selected sintering parameters that were registered during the SPS process, as a function of the process time: temperature, force, and punch displacement.

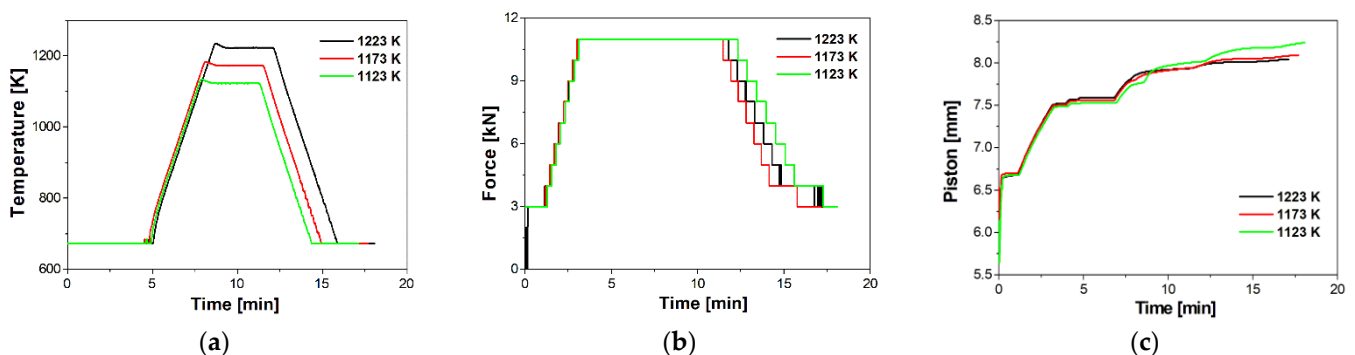


Figure 3. Actual (a) temperature-time, (b) force-time, and (c) punch displacement-time curves registered during SPS.

2.3. Material Characterisation

The density of the sintered composites was measured by Archimedes' principle. Relative density is the ratio of measured density to theoretical density. An analytical balance

RADWAG AS 220/C/2 (Radwag, Radom, Poland) was used to measure the weight of the samples. Young's modulus was determined using the Panametrics Epoch III flaw detector (Panametrics, Billerica, MA, USA). Young's modulus was measured based on the velocity of ultrasonic waves transition through the sinter. The velocities of the transverse and longitudinal waves were calculated as the ratio of sample thickness to relevant transition time. For each sample, five measurements of Young's modulus were performed. The measurement error was 2%.

The NEXUS 4000 microhardness tester (Innovatest EuropeBV, Maastricht, The Netherlands) was used to measure the average hardness of the composites at the load of 2.942 N and a hold time of 10 s. Each sample was tested with 10 points.

X-ray diffraction analysis (XRD) was carried out using a diffractometer equipped with a Cu/K α radiation. The microstructures of the sintered composites were evaluated using scanning electron microscopy (JEOL JSM 6610LV, Tokyo, Japan) equipped with energy-dispersive spectroscopy (EDS, Aztec, Oxford Instruments, High Wycombe, UK).

The electrical conductivity of the samples was determined according to the diagram in Figure 4 using the four-point method [49,50]. The measurement system used a 2182A 2-channel nanovoltmeter (Tektronix UK Ltd., Berkshire, UK) and a precision Array Electronic 3644A programmable power supply 18 V/5 A (Array Electronic Co. Ltd., Nanjing, China). The current flowing in the measurement circuit did not exceed 0.5 A. This allowed us to avoid heating of the sample during measurement. Each single measurement was performed as the average of two results obtained with different polarisations. Five measurements were made in each sample variant and the results were averaged.

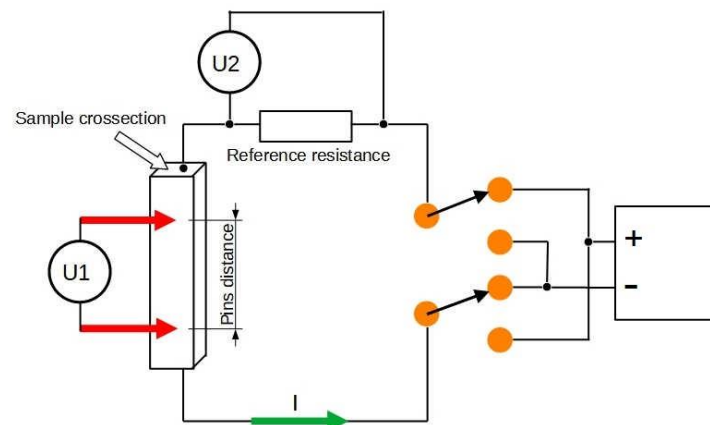


Figure 4. Schematic of the electrical conductivity measurement station.

3. Research Results

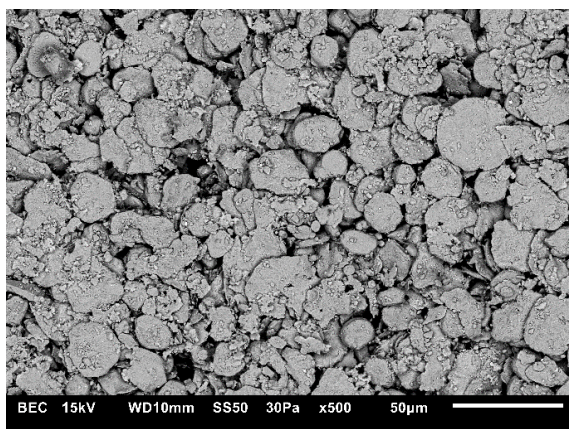
3.1. Characterisation of Composite Powder Mixtures

The changes in the shape and size of the powder particles that occurred during milling were analysed using a scanning electron microscope and a nano analyser. The microstructures and particle size distributions of composite powders containing 5 wt% ZrB₂ milled for 5, 10, 15, and 20 h, respectively, are shown in Figures 5–8. The starting copper powder was characterised by a spherical shape and an average particle size of 10 μm (Figure 1). The ZrB₂ powder particles were shaped like polyhedra with sharp edges (Figure 2). The use of the milling process resulted in a change in the morphology and size of the composite powders. After 5 h of milling (Figure 5), the composite powder particles flattened. There was an increase in particle size (Figure 5b, Table 3) to approximately 17 μm . In the initial stage of the milling process, powder particles were subjected to high-energy collisions, which caused plastic deformation. This led to a strengthening of the particles and subsequent cracking. As a result of cracking, new surfaces were created, which allowed the powder particles to bond with each other [51,52]. The consequence of the bonding process was the growth of the composite powder particles in relation to the particle size

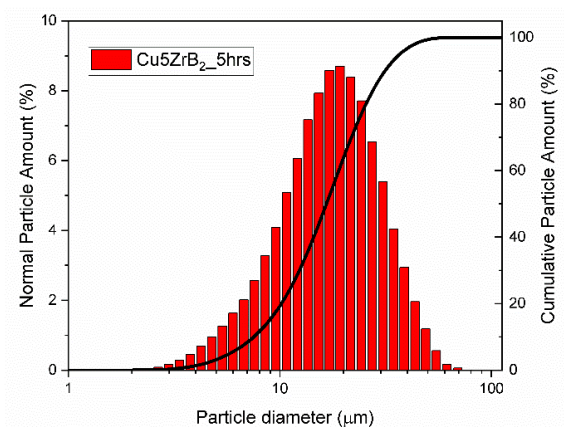
of the initial copper powder (Figure 5). In the subsequent stages of milling (after 10, 15, and 20 h), the matrix powder particles were further deformed (Figures 6–8), and hard reinforcement particles became fragmented due to severe plastic deformation. As a result, the particle size of the composite powder gradually decreased as a function of the milling time (Table 3). After 20 h of milling, the average particle size of the composite powder with 5 wt% ZrB₂ was approximately 13 μm (Figure 8). The powder particles had a flake shape with a developed and wrinkled surface. Analogous changes in the shape of the powders were observed as a function of the milling time (5–20 h) for other composite mixtures containing 10, 15, and 20 wt% ZrB₂.

Table 3. Results of the particle size distribution of powders after different milling times.

Powders	Median D (μm)	Modal D (μm)
Cu + 5ZrB ₂ (5 h)	16.587	17.138
Cu + 5ZrB ₂ (10 h)	17.677	21.633
Cu + 5ZrB ₂ (15 h)	17.304	20.952
Cu5 + ZrB ₂ (20 h)	11.752	13.277

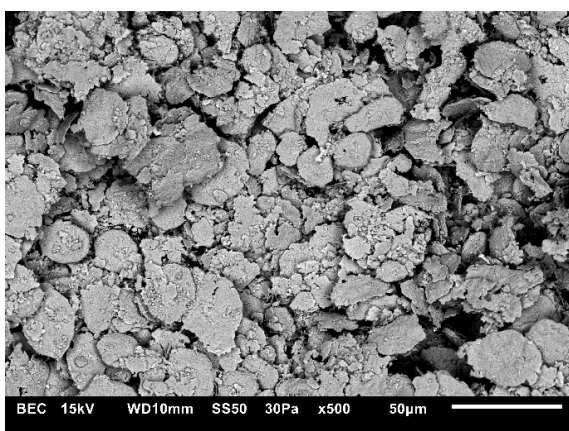


(a)

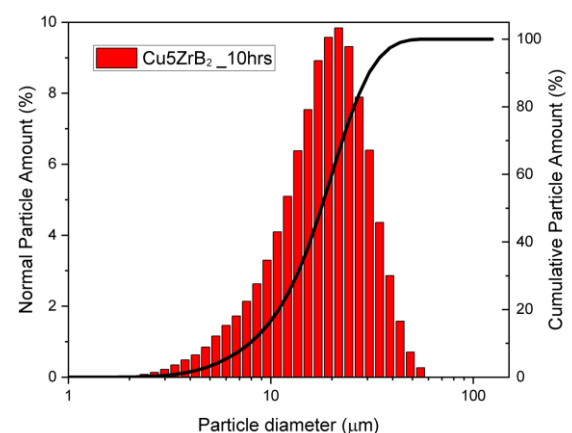


(b)

Figure 5. (a) Microstructure (SEM) and (b) particle size distribution of the powders with 5% ZrB₂ after 5 h.

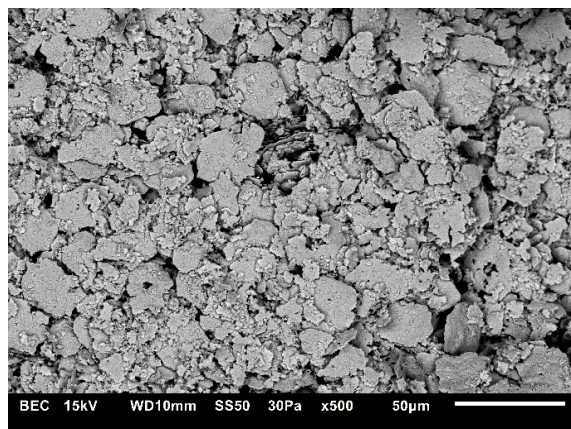


(a)

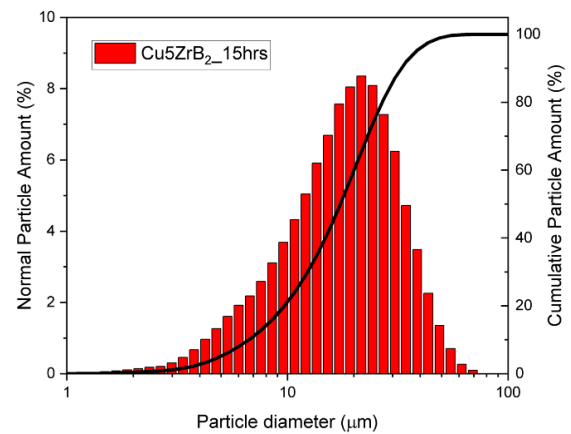


(b)

Figure 6. (a) Microstructure (SEM) and (b) particle size distribution of the powders with 5% ZrB₂ after 10 h.

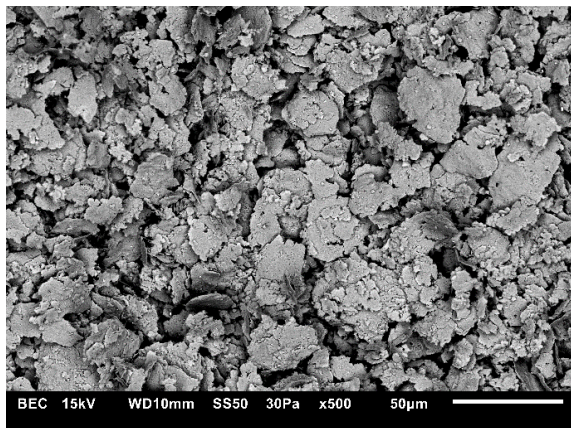


(a)

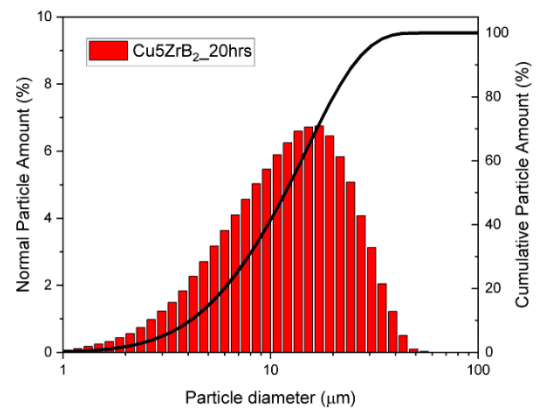


(b)

Figure 7. (a) Microstructure (SEM) and (b) particle size distribution of the powders with 5% ZrB₂ after 15 h.



(a)



(b)

Figure 8. (a) Microstructure (SEM) and (b) particle size distribution of the powders with 5% ZrB₂ after 20 h.

Furthermore, the results of testing the composite mixtures (Figure 9) showed that changing the amount of the reinforcement phase had a beneficial effect on the particle size distribution. After 20 h of milling, a decrease in the average particle size of the powders was observed with an increase in the amount of ZrB₂. For comparison, the average particle size of the composite powder was approximately 13 µm, 11.5 µm, 7 µm, and 5 µm for contents of 5, 10, 15, and 20 wt% ZrB₂, respectively (Table 4). During the milling process, the Cu powder tended to cold-weld together, while the brittle and hard ZrB₂ particles would fragment. In this case, zirconium diboride can act as a milling aid, especially when its amount in the Cu matrix increases [53]. Figure 10 shows a comparison of the results of X-ray analyses of composite powders containing 5% ZrB₂ after selected milling times. The diffraction peaks of copper and ZrB₂ are clearly visible in the X-ray recording of the composite powders after each milling stage (5–10–15–20 h). They also revealed the presence of small amounts of CuZr and Zr phases in the powder mixtures. Similar test results were obtained for all composite powders. No changes in the intensity of the peaks originating from Cu, ZrB₂, Zr, and CuZr were observed in the diffractograms as the milling time increased.

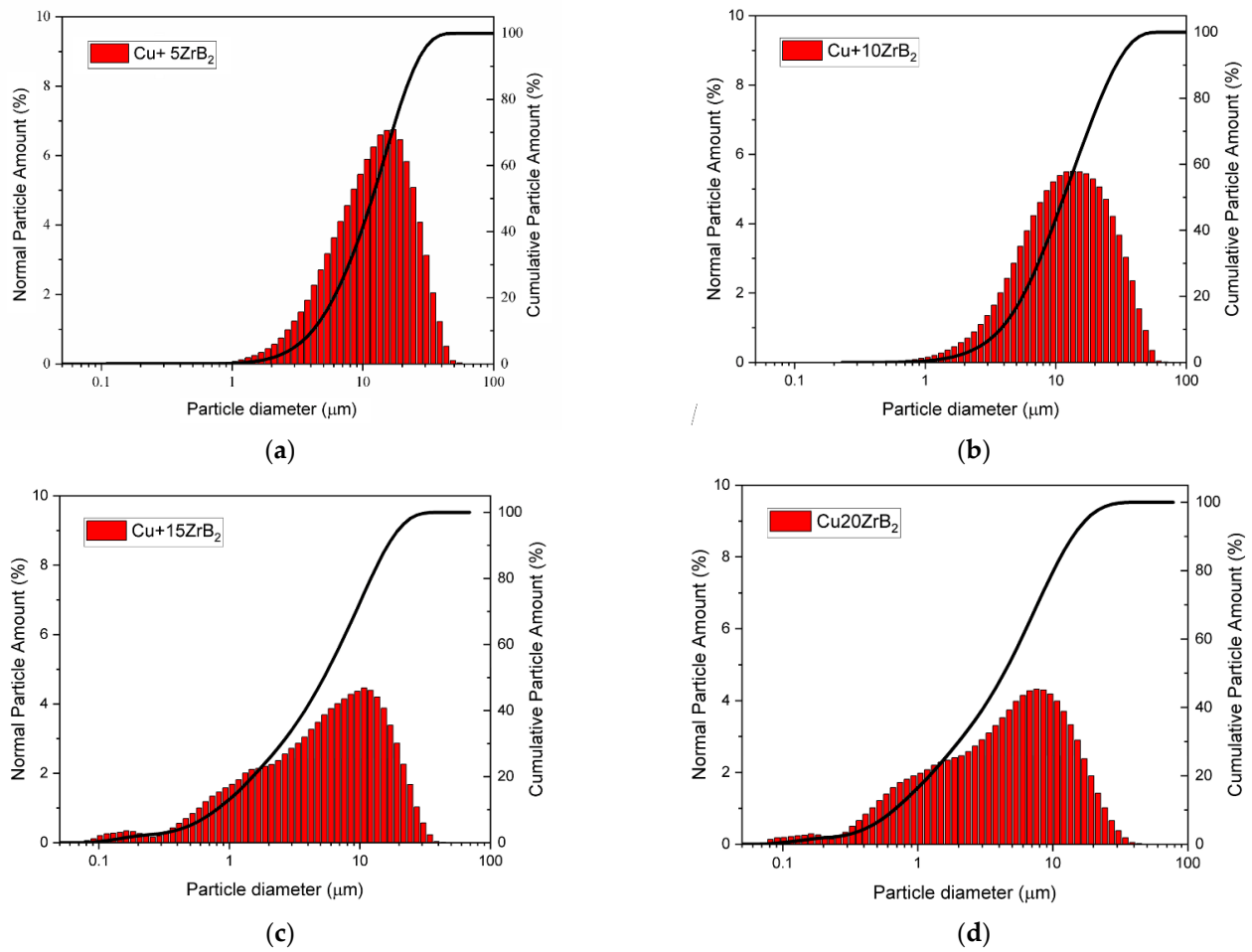


Figure 9. Comparison of the particle size of powders with different ZrB₂ contents (a–d).

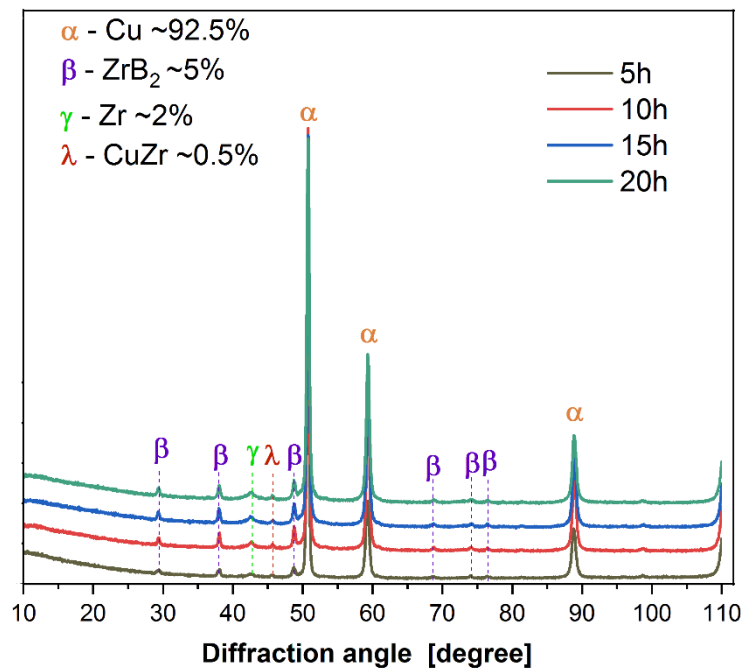


Figure 10. XRD pattern of the Cu + 5ZrB₂ powders milled for different times.

Table 4. Results of particle size distribution of powders with different ZrB₂ contents.

Powders	Median D (μm)	Modal D (μm)
Cu + 5ZrB ₂	11.752	13.277
Cu + 10ZrB ₂	10.308	11.556
Cu + 15ZrB ₂	4.454	6.750
Cu5 + 20ZrB ₂	3.402	5.348

3.2. Characterisation of Sintered Cu–ZrB₂ Composites

The parameters of the SPS process play a significant role in shaping the properties of the sintered materials. Therefore, in the first stage of the research, optimisation of the sintering conditions was carried out. Sintered Cu–ZrB₂ composites were evaluated in terms of the degree of compaction (density and porosity) to indicate optimal sintering conditions. An additional parameter taken into account in the optimisation of the sintering conditions was the value of Young’s modulus determined using the ultrasonic method. The results of the tests on the influence of the sintering pressure and temperature on the properties analysed are presented in Tables 5 and 6. Composites sintered at temperatures of 1123 K, 1173 K, and 1223 K at a pressure of 20 MPa were characterised by low relative density (84–89%), high porosity (11.34–6.95%) and low Young’s modulus values (88–106 GPa). The high porosity of the sintered material indicates the presence of defects and inhomogeneities in the material, which may affect the attenuation of ultrasonic waves during measurements and obtain low values of Young’s modulus [54,55]. Increasing the sintering pressure to 35 MPa resulted in a high degree of densification. The relative density of the sintered composites was in the range of 95–97% (Table 5), and the open porosity decreased to 1.12–2.54%. Similarly, higher values of Young’s modulus were obtained. The test results showed (Table 6) that very similar values of density, open porosity, and Young’s modulus were determined for copper without a reinforcing phase, which was sintered at temperatures of 1123–1223 K. These results recommend performing the SPS process for pure copper at a lower temperature of 1123 K. However, in the case of Cu–ZrB₂ composites, the temperatures of 1123 K and 1173 K are insufficient to obtain a high degree of densification. The negative effect of these sintering conditions was particularly clearly observed for Table 6 (the influence of the sintering pressure on the properties of the materials formed by SPS).

Table 5. Influence of the sintering pressure on the properties of the materials formed by SPS.

Sintered Materials	Temperature [K]	Pressure [MPa]	Apparent Density [g/cm ³]	Relative Density [%]	Open Porosity [%]	Young’s Modulus [GPa]	Relative Young’s Modulus [%]
Cu + 5%ZrB ₂	1123	20	7.45	84	11.34	88	68
	1173		7.68	87	9.89	92	72
	1223		7.89	89	6.95	106	82
	1123	35	8.35	95	2.54	113	88
	1173		8.46	96	1.78	117	91
	1223		8.52	97	1.12	123	97

Table 6. Influence of the sintering temperature on the properties of the materials formed by SPS.

Sintered Materials	Temperature [K]	Apparent Density [g/cm ³]	Relative Density [%]	Open Porosity [%]	Young's Modulus [GPa]	Relative Young's Modulus [%]
Cu	1123	8.75	98	0.12	107	97
	1173	8.74	98	0.13	107	97
	1223	8.76	98	0.12	105	98
Cu + 5%ZrB ₂	1123	8.35	95	2.54	113	88
	1173	8.46	96	1.78	117	91
	1223	8.52	97	1.12	123	97
Cu + 10%ZrB ₂	1123	7.62	88	9.78	112	76
	1173	7.94	92	3.18	126	85
	1223	8.18	94	1.89	139	96
Cu + 15%ZrB ₂	1123	7.41	87	10.67	119	71
	1173	7.53	88	8.71	132	79
	1223	7.86	92	3.21	154	94
Cu + 20%ZrB ₂	1123	7.22	86	10.54	129	72
	1173	7.31	87	9.73	143	80
	1223	7.57	90	3.83	165	93

Meanwhile, increasing the temperature of the SPS process to 1223 K improved the density of the composites and porosity, and increased Young's modulus. For this sintering temperature, the highest values of relative density above 90%, low porosity, and a higher Young's modulus in the range (92–96%) were achieved. Increasing the sintering temperature is beneficial because a higher temperature accelerates atomic diffusion and increases the migration rate of grain boundaries, which in turn promotes a reduction of pore size and an improvement in density [56,57]. This is consistent with the results of other works [33,58,59]. Wang et al. [33] investigated the effect of the SPS process temperature at a pressure of 40 MPa on the properties of Cu–TiC composites. They showed that increasing the temperature of the SPS process improved the relative density of sintered materials. Soloviova et al. [58] demonstrated similar correlations for Cu–(LaB₆-TiB₂) composites also prepared using the SPS method.

Analysis of the results indicated a characteristic dependence of the properties of sintered composites as a function of the change in the amount of the ZrB₂-reinforcing phase (Figures 11 and 12, Table 6). The apparent density of the composites decreased from 8.52 g/cm³ to 7.57 g/cm³ with an increase in the content of ZrB₂ (5–20%). The reduction in the density of the composites is mainly due to the lower density of ZrB₂ ceramics (6.10 g/cm³) compared to copper (8.96 g/cm³) [28,60,61]. Wang et al. [23] observed a similar trend in their research. They produced Cu–ZrB₂ composites using a hot-pressing sintering process at a temperature of 840 °C and a pressure of 25 MPa. A decrease in density was found (from 96.1 to 91.3%) when the ZrB₂ content was changed (1–9 wt%). The test results showed that the Young's modulus increased with the increase in the ZrB₂ content in the copper matrix (Figure 12). The values of Young's modulus were 105 GPa, 123 GPa, 139 GPa, 154 GPa, and 165 GPa (Table 6) for sintered copper and composites with 5 wt%, 10 wt%, 15 wt%, and 20 wt% ZrB₂, respectively. The introduction of 20 wt% ZrB₂ into the copper matrix resulted in an increase in the value of Young's modulus by approximately 60% compared to sintered copper without a reinforcing phase. Hardness also showed a positive correlation with the change in ZrB₂ content (Figure 13). Furthermore, only the addition of 5 wt% ZrB₂ increased the hardness twice compared to pure copper. Increasing the ZrB₂ content had a beneficial effect on improving hardness. Composites containing

20 wt% ZrB₂ were characterised by 3x higher hardness (174 HV0.3) compared to sintered copper (61 HV0.3). This is the result of the presence of the ZrB₂ reinforcement phase in the copper matrix, which has a very high hardness (>2200 HV [58]). The improvement of microhardness can be explained by the uniform distribution of ZrB₂ particles within the Cu matrix. Wang et.al. [23] reported that the microhardness of the pure copper (57.5 HV0.2) increased to 100.8 HV0.2 with increasing ZrB₂ content up to 7 wt%.

Microstructural studies with chemical composition (EDS) and phase composition (X-ray diffraction) analyses were carried out for all sintered Cu–ZrB₂ composites. For comparison, Figures 14 and 15 show exemplary microstructures of Cu–10 wt% ZrB₂ and Cu–20 wt% ZrB₂ composites. A uniform distribution of the reinforcing phase was observed in the copper matrix. Only for composites containing 20 wt% ZrB₂, the local formation of ZrB₂ agglomerates was demonstrated (Figure 15). Phase analyses (Figure 16) confirmed the presence of only the ZrB₂ and copper phase for all sintered composites.

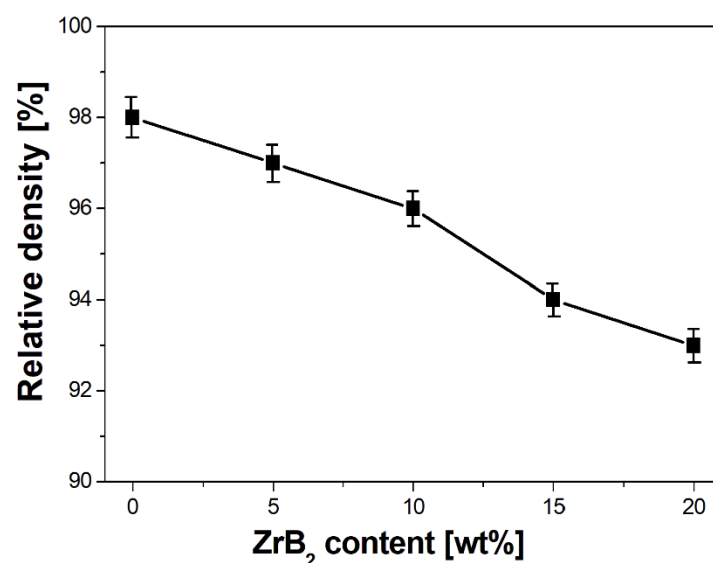


Figure 11. Effect of the ZrB₂ content on the density of sintered materials (temperature 1223 K).

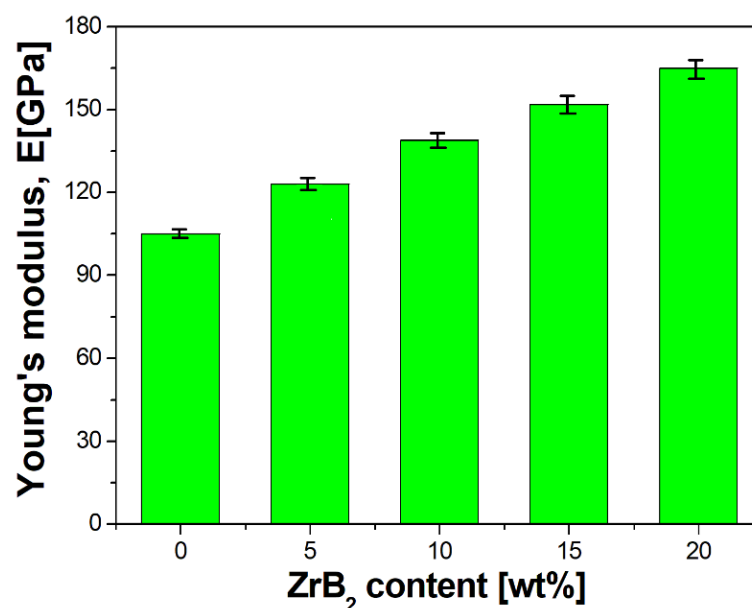


Figure 12. Effect of the ZrB₂ content on Young's modulus (temperature 1223 K).

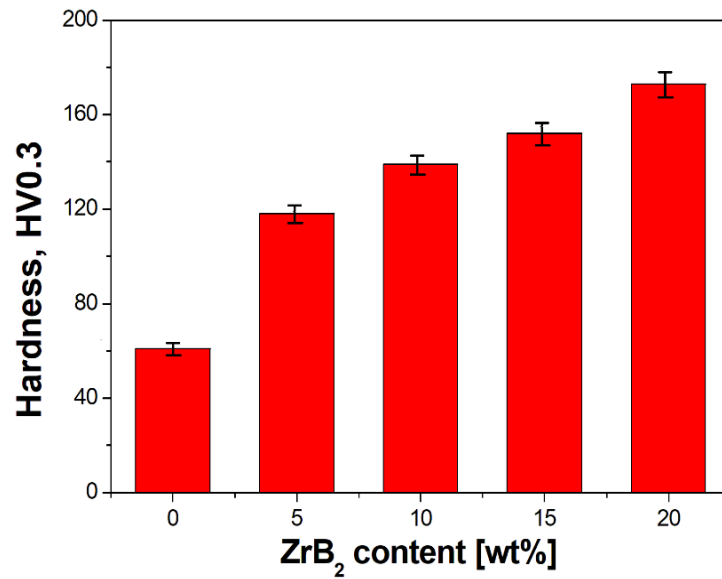


Figure 13. Effect of the ZrB₂ content on the hardness of sintered materials.

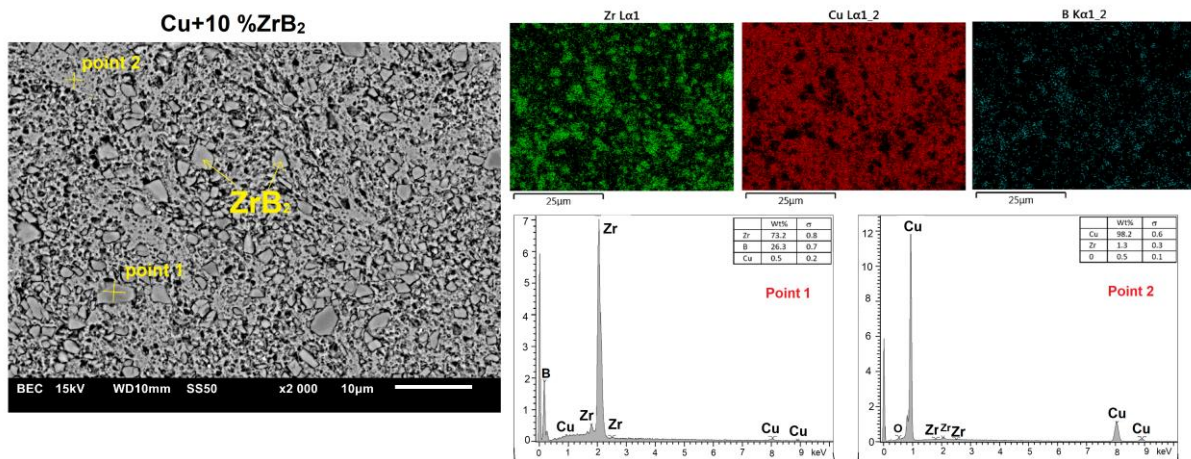


Figure 14. The microstructure (SEM) of Cu + 10%ZrB₂ composite with the corresponding point analysis and area analysis (WDS).

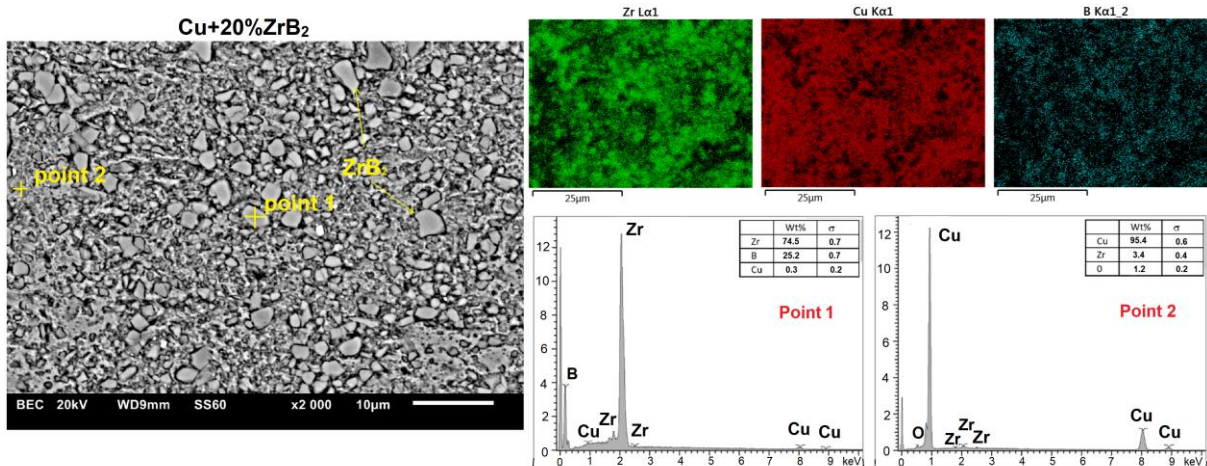


Figure 15. The microstructure (SEM) of Cu + 20%ZrB₂ composite with the corresponding point analysis and area analysis (WDS).

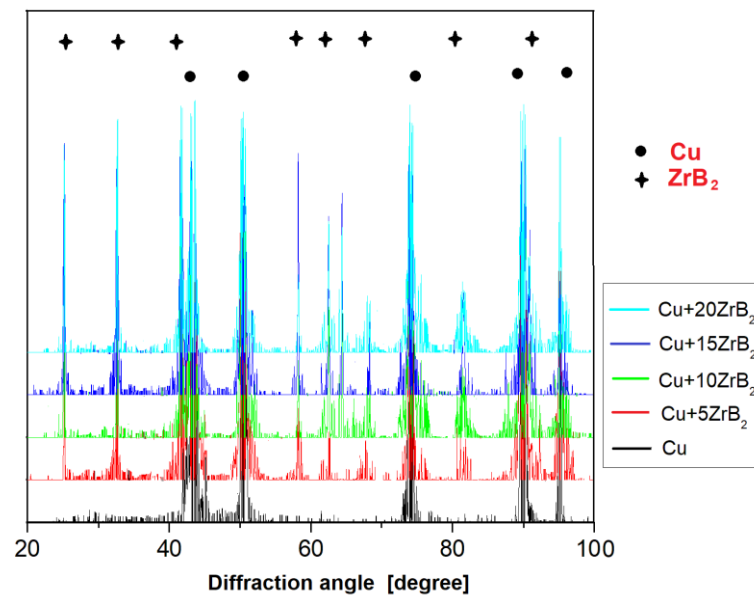


Figure 16. X-ray diffraction patterns of composites after the SPS process at a sintering temperature of 1223 K and a pressure of 35 MPa.

Comparisons of relative electrical conductivity for sintered materials are presented in Figure 17. The results obtained were related to the conductivity of pure electrolytic copper ([62]), whose value was taken as 100%. The addition of ZrB_2 caused a strong decrease in the electrical conductivity of the composites. The effect was most visible with 10% of the content of the reinforcement phase and more. This was caused by a sharp reduction in the share of pure copper in the active cross section of the material. The observed decrease amount and its subsequent stabilisation at a constant level may indicate partial diffusion of the components from zirconium diboride into the copper matrix. According to [63], the solubility of Zr in copper at room temperature is negligible; however, the content of boron dissolved in the structure can be up to 0.06 at% [64]. Such a disturbance at the level of the matrix structure combined with discontinuities resulting from sintering may have a significant impact on the electrical properties and cause the observed effects.

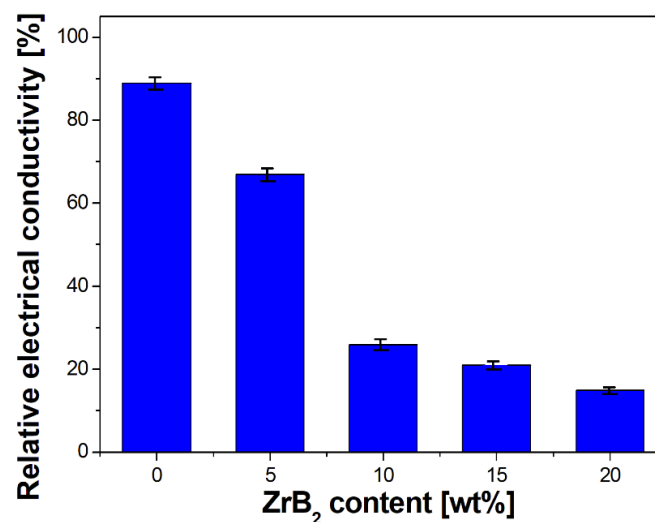


Figure 17. Effect of the ZrB_2 content on the relative electrical conductivity of sintered materials. A value of 100% conductivity corresponds to pure electrolytic copper, while the bars shown reflect the decrease in electrical performance associated with obtaining composite with different contents of ZrB_2 (from 0 to 20 wt%) by SPS technology.

4. Discussion

The preparation of composite powders by milling is of key importance for the properties of the material produced in the SPS process. It was observed that during the milling process, the amount of the added reinforcing phase affects the distribution of the particles in the copper matrix. During milling, the higher content of ZrB₂ in the composite powders improves the uniformity of particle distribution. Moreover, the particle size distribution curve undergoes favourable changes, which tends toward an ideal Gaussian curve without a clear maximum. This effect is especially visible for the content of 5 and 10 wt% ZrB₂ (Figure 9a,b). Increasing the content of ZrB₂ in powder mixtures results in the appearance of a significant number of fine particles resulting from the kinetics of the milling process. However, they do not disturb the homogeneous distribution of the reinforcing phase in the matrix.

Furthermore, during the milling process, an initial mechanical synthesis is carried out, resulting in the CuZr phase observed in composite mixtures and a small fraction of pure zirconium particles released from the ZrB₂ phase. The results of the diffraction analysis (Figure 10) show that the synthesis process of these phases takes place after 5 h of milling. Extending the milling time to 20 h does not affect the formation of subsequent phases, but only affects the number of previously identified ones, as evidenced by the observed changes in the intensity of individual peaks on the graph. The sintered composite material shows a linear dependence of density (Figure 11) and Young's modulus (Figure 12) on the amount of the reinforcing phase. A similar relationship was observed for microhardness measurements (Figure 13). The linear characteristics of these parameters indicate the homogeneity of the material and allow for good predictions of parameters when using other proportions. The results also show that in the case of the highest ZrB₂ content (20 wt%), the formation of conglomerates of ZrB₂ particles can be observed. This is an unfavourable phenomenon and may indicate microstructure homogeneity problems for ZrB₂ contents of 20 wt% and above. The phase analysis of the sintered composites (Figure 16) showed in all cases the existence of only two phases, i.e., the copper matrix and ZrB₂. The small amounts of Zr and ZrCu phases observed in powder mixtures after mechanical synthesis disappeared as a result of the diffusion processes accompanying the sintering.

The electrical conductivity of composites containing metal borides is reduced due to changes in the proportions of components with different electrical properties in the cross-section of the sample. In the case of materials with small (short-range) diffusion exchange of components, it should be proportional to the volume fraction of the reinforcing phase. However, for solution hardening materials, where alloy addition occurs evenly throughout the matrix and modifies the parameters of the crystal lattice by introducing more point defects and, consequently, conduction electron scattering centres, even a small amount of the addition may cause a significant decrease in the electrical conductivity of the material.

A similar relationship occurs for thermal conductivity, which has a different nature in terms of the conduction mechanism. However, both mechanisms share common macroscopic features that can be expressed by a general transport equation. They are a generalisation of Ohm's law for the density of electric current (current flux— j) in a conductor:

$$j = \sigma E \quad (1)$$

where:

σ —electrical conductivity tensor,
 E —vector of electric field intensity,
 and

Fourier's law describing the amount of thermal energy flow q :

$$q = -\kappa_x (dT/dx) \quad (2)$$

where:

κ_x —thermal conductivity coefficient along the x axis,

dT/dx —temperature gradient.

Both E and dT/dx have a gradient character, so in general we can write:

$$j = -\beta \cdot \text{grad}A \quad (3)$$

where:

j —flux density vector of the appropriate amount (size) of internal energy for thermal conduction or charge for electrical conduction,

β —coefficient of proportionality of thermal or electrical conductivity,

A —scalar quantity whose gradient causes a given phenomenon (temperature, electric potential) [64].

In the case of the sintered Cu–ZrB₂ composite, the results indirectly indicate the partial diffusion of boron into the copper matrix, which may explain the observed strong decrease in the electrical conductivity of the samples with the increase in the content of the ZrB₂ phase. The easy diffusion transfer to the matrix results from the large difference in the atomic radius of copper (140 pm) and boron (85 pm). This means that boron will tend to be located in the interstitial holes of the copper lattice and cause local contraction of the crystal lattice, increasing the scattering potential of conduction electrons. At the same time, as shown by [65], the limit of solubility of boron in copper does not exceed 0.06% at room temperature. A strong initial drop in conductivity and then its stabilisation may indicate that boron has diffused into the matrix and reached limiting solubility.

5. Conclusions

1. A change in SPS temperature from 1123–1223 K led to an increase in the density, Young's modulus, and hardness. The best physical and mechanical properties were obtained for the composites that were sintered at 1223 K–35 MPa.
2. Furthermore, the influence of the ZrB₂ content on the microstructure, physical, mechanical, and electrical properties of sintered composites was studied. The results showed that the increase in the ZrB₂ content in the copper matrix improves Young's modulus and hardness while reducing the density and electrical conductivity. The addition of the reinforcing phase in an amount greater than 10 wt% negatively affects the properties of the copper matrix composites.
3. The addition of 20 wt% ZrB₂ causes the beginning of the formation of particle conglomerates and, consequently, disturbs their homogeneous distribution in the copper matrix.
4. A strong decrease in the electrical conductivity of composites containing 5 and 10 wt% ZrB₂, as well as stabilization of the conductivity in larger amounts, indicates the partial diffusion of boron into the copper matrix.

Author Contributions: Methodology, I.S. and G.B.; Formal analysis, I.S.; Investigation, I.S. and G.B.; Writing—original draft, I.S. All authors have read and agreed to the published version of the manuscript.

Funding: This research was funded by funds of the Institute of Technology, University of the National Education Commission (WPBU/2023/03/00001). The project for the purchase of scientific and research equipment: "Innovative research and scientific platform for a new class of nanocomposites", financed by the Ministry of Education and Science, contract number 7216/IA/SP/2021.

Institutional Review Board Statement: Not applicable.

Informed Consent Statement: Not applicable.

Data Availability Statement: The data presented in this study are available on request from the corresponding author.

Conflicts of Interest: The authors declare no conflict of interest.

References

1. Renwick, S. Copper Alloys: Processes, Applications and Developments. In *Copper and Copper Base Alloys: The Physical and Mechanical Properties of Copper and Its Commercial Alloys in Wrought Form*; Forgotten Books; New York Research Press: New York, NY, USA, 2018.
2. Wang, Q.; Chen, M.; Shan, Z.; Sui, C.; Zhang, L.; Zhu, S.; Wang, F. Comparative study of mechanical and wear behavior of Cu/WS₂ composites fabricated by spark plasma sintering and hot pressing. *J. Mater. Sci. Technol.* **2017**, *33*, 1416–1423. [[CrossRef](#)]
3. Zhou, D.S.; Zhang, D.L.; Kong, C.; Munroe, P. Factors controlling the tensile properties of ultrafine structured Cu–5vol%Al₂O₃ nanocomposite prepared by high energy mechanical milling and powder compact extrusion. *Mater. Sci. Eng. A* **2013**, *584*, 67–72. [[CrossRef](#)]
4. Kim, J.H.; Yun, J.H.; Park, Y.H.; Cho, K.M.; Choi, I.D.; Park, I.M. Manufacturing of Cu-TiB₂ composites by turbulent in situ mixing process. *Mater. Sci. Eng. A* **2007**, *449–451*, 1018–1021. [[CrossRef](#)]
5. Shi, Y.; Chen, W.; Dong, L.; Li, H.; Fu, Y. Enhancing copper infiltration into alumina using spark plasma sintering to achieve high performance Al₂O₃/Cu composites. *Ceram. Int.* **2018**, *44*, 57–64. [[CrossRef](#)]
6. Zhang, Y.; Ji, Z.; Jia, C.; Liu, G.; Wan, F.; Zhan, Q. Influence of lanthanum on enhancement of mechanical and electrical properties of Cu–Al₂O₃ composites. *J. Rare Earths* **2019**, *37*, 534–540. [[CrossRef](#)]
7. Efe, G.C.; Altinsoy, I.; Yener, T.; Ipek, M.; Zeytin, S.; Bindal, C. Characterization of cemented Cu matrix composites reinforced with SiC. *Vacuum* **2010**, *85*, 643–647. [[CrossRef](#)]
8. Aal, M.I.A.E. Effect of high-pressure torsion processing on the microstructure evolution and mechanical properties of consolidated micro size Cu and Cu–SiC powders. *Adv. Powder Technol.* **2017**, *28*, 2135–2150. [[CrossRef](#)]
9. Yu, Z.; Zhu, H.; Huang, J.; Li, J.; Xie, Z. Processing and characterization of in-situ ultrafine TiB₂–Cu composites from Ti–B–Cu system. *Powder Technol.* **2017**, *320*, 66–72. [[CrossRef](#)]
10. Ruzic, J.; Stasic, J.; Rajkovic, V.; Bozic, D. Synthesis, microstructure and mechanical properties of ZrB₂ nano and microparticle reinforced copper matrix composite by in situ processing's. *Mater. Des.* **2014**, *62*, 409–415. [[CrossRef](#)]
11. Kumari, S.; Kumar, A.; Sengupta, P.R.; Dutta, P.K.; Mathur, R.B. Improving the mechanical and thermal properties of semi-coke based carbon/copper composites reinforced using carbon nanotubes. *Adv. Mater. Lett.* **2014**, *5*, 265–271. [[CrossRef](#)]
12. Yang, L.; Sun, L.; Bai, W.; Li, L. Thermal conductivity of Cu–Ti/diamond composites via spark plasma sintering. *Diam. Relat. Mater.* **2019**, *94*, 37–42. [[CrossRef](#)]
13. Jiang, Y.; Wang, D.; Xu, Y.; Cao, F.; Liang, S. Fabrication and properties of in situ heterogeneous Cu/TiB₂ composites with a harmonic structure. *Mater. Lett.* **2020**, *263*, 127–132. [[CrossRef](#)]
14. Xie, J.; Zeng, W.; Zhou, D.; Zhang, D. Microstructure and properties of a nanocrystalline Cu–Al–NbC composite with high strength and good conductivity. *Mater. Lett.* **2018**, *214*, 174–177. [[CrossRef](#)]
15. Gao, X.; Yue, H.; Guo, E.; Zhang, H.; Lin, X.; Yao, L.; Wang, B. Mechanical properties and thermal conductivity of graphene reinforced copper matrix composites. *Powder Technol.* **2016**, *301*, 601–607. [[CrossRef](#)]
16. Cho, H.J.; Kim, Y.J.; Erb, U. Thermal conductivity of copper–diamond composite materials produced by electrodeposition and the effect of TiC coatings on diamond particles. *Compos. Part B* **2018**, *155*, 197–203. [[CrossRef](#)]
17. Safari, F.; Khosroshahi, R.A.; Zolriasatein, A. Wear behavior of copper matrix composites reinforced by γ -Cu₅Zn₈ nanoparticles. *Powder Technol.* **2017**, *318*, 549–557. [[CrossRef](#)]
18. Prajapati, P.K.; Chaira, D. Fabrication and characterization of Cu–B₄C metal matrix composite by powder metallurgy: Effect of B₄C on microstructure, mechanical properties and electrical conductivity. *Transit. Indian Inst. Met.* **2018**, *72*, 673–684. [[CrossRef](#)]
19. Monteverde, F.; Belloni, A.; Guicciardi, S. Processing and properties of zirconium diboride-based composites, *The Journal of the European. Ceram. Soc.* **2002**, *22*, 279–288. [[CrossRef](#)]
20. Wilkins, J.M.L. *Boron and Refractory Borides*; Matkovich, V.I., Ed.; Springer: New York, NY, USA, 1977; p. 633.
21. Mroz, C. Zirconium diboride. *J. Am. Ceram. Soc. Bull.* **1994**, *73*, 141–142.
22. Fan, X.; Liu, Q.; Ding, H.; Wang, H.; Hao, C. The microstructures and properties of in-situ ZrB₂ reinforced Cu matrix composites. *Results Phys.* **2019**, *14*, 102494. [[CrossRef](#)]
23. Wang, C.; Lin, H.; Zhang, Z.; Li, W. Fabrication, Interfacial characteristics and strengthening mechanisms of ZrB₂ microparticles reinforced Cu composites prepared by hot-pressed sintering. *J. Alloys Compd.* **2018**, *748*, 546–552. [[CrossRef](#)]
24. Guan, C.; Chen, G.; Kai, X.; Gao, X.; Huang, L.; Cao, R.; Qian, W.; Zhao, Y. Transformation of dislocation strengthening mechanisms induced by graphene nanoplates and ZrB₂ nanoparticle in nanolaminated Al matrix composites. *Powder Technol.* **2021**, *377*, 723–732. [[CrossRef](#)]
25. Rino, J.J.; Prabu, S.B.; Paskaramoorthy, R. Comparison of thermal and mechanical properties of Al-5wt.%TiB₂ and Al-5wt.%ZrB₂ composites processed through salt-melt reaction route. *Mater. Today Proc.* **2017**, *8*, 8739–8750. [[CrossRef](#)]
26. Çamurlu, H.E.; Maglia, F. Self-propagating high-temperature synthesis of ZrB₂ or TiB₂ reinforced Ni–Al composite powder. *J. Alloys Compd.* **2009**, *478*, 721–725. [[CrossRef](#)]
27. Jiang, S.; An, Q.; Cui, X.; Xiang, X.; Huang, L.; Zhang, R.; Sun, Y.; Geng, L. Fabrication and mechanical properties of the titanium matrix composites based on Ti₆Al₄V–ZrB₂–(Si) system. *Mater. Sci. Eng. A* **2021**, *819*, 141488. [[CrossRef](#)]
28. Davis, J.R. *Copper and Copper Alloy*; ASM International: Materials Park, OH, USA, 2001.
29. Ding, H.; Miao, W.; Huang, X.; Liu, Q.; Fan, X.; Wang, H.; Chu, K.; Li, C. Influence of Al addition on microstructures of Cu–B alloys and Cu–ZrB₂ composites. *Trans. Nonferrous Met. Soc. China* **2020**, *30*, 1335–1346. [[CrossRef](#)]

30. Shaik, M.A.; Golla, B.R. Two body abrasion wear behaviour of Cu–ZrB₂ composites against SiC emery paper. *Wear* **2020**, *450–451*, 203260. [[CrossRef](#)]
31. Zhang, P.; Wang, C.; Zhou, S.; Guo, B.; Zhang, Z.; Yu, Z.; Li, W. Effect of sintering temperature of the microstructure and properties of high-strength and highly conductive 5 wt.% ZrB₂/Cu composite. *Powder Metall. Met. Ceram.* **2023**, *61*, 9–10.
32. Zhang, X.; Qian, L.; Bin, L.; Xi, C.; You, L.; Zhen, H.; Huan, L. Enhanced softening resistance and mechanical properties of Mo₂C particle-reinforced Cu-matrix composites. *Compos. Struct.* **2023**, *305*, 116503. [[CrossRef](#)]
33. Wang, F.; Li, Y.; Wang, X.; Koizumi, Y.; Kenta, Y.; Chiba, A. In-situ fabrication and characterization of ultrafine structured Cu-TiC composites with high strength and high conductivity by mechanical milling. *J. Alloys Compd.* **2016**, *657*, 122–132. [[CrossRef](#)]
34. Dash, K.; Ray, B.C.; Chaira, D. Synthesis and characterization of copper–alumina metal matrix composite by conventional and spark plasma sintering. *J. Alloys Compd.* **2012**, *516*, 78–84. [[CrossRef](#)]
35. Hyjek, P.; Stepień, M.; Kowalik, R.; Sulima, I. Corrosion Resistance of Nickel-Aluminum Sinters Produced by High-Pressure HPHT/SPS Method. *Materials* **2023**, *16*, 1907. [[CrossRef](#)] [[PubMed](#)]
36. Zhu, Y.; Qin, J.; Wang, J.; Jin, P.; Li, P. Significant strain hardening ability of AZ91 magnesium alloy fabricated by spark plasma sintering. *Mater. Today Commun.* **2023**, *35*, 105670. [[CrossRef](#)]
37. Venkateswaran, T.; Basu, B.; Raju, G.B.; Kim, D.Y. Densification and properties of transition metal borides-based cermets via spark plasma sintering. *J. Eur. Ceram. Soc.* **2006**, *26*, 2431–2440. [[CrossRef](#)]
38. Shi, X.; Shao, G.; Duan, X.; Yuan, R. Study on the diamond/ultrafine WC-Co cermets interface formed in a SPS consolidated composite. *Rare Met.* **2006**, *25*, 150–155. [[CrossRef](#)]
39. Chakraborty, S.; Mallick, A.R.; Debnath, D.; Das, P.K. Densification, mechanical and tribological properties of ZrB₂ by SPS, Effect of pulsed current. *Int. J. Refract. Met. Hard Mater.* **2015**, *4*, 150–156. [[CrossRef](#)]
40. Hocquet, S.; Dupont, V.; Cambier, F.; Ludewig, F.; Vandewalle, N. Densification of complex shape ceramics parts by SPS. *J. Eur. Ceram. Soc.* **2020**, *40*, 2586–2596. [[CrossRef](#)]
41. Sulima, I.; Putyra, P.; Hyjek, P.; Tokarski, T. Effect of SPS parameters on densification and properties of steel matrix composites. *Adv. Powder Technol.* **2015**, *26*, 1152–1161. [[CrossRef](#)]
42. Fujii, T.; Tohgo, K.; Iwao, M.; Shimamura, Y. Fabrication of alumina-titanium composites by spark plasma sintering and their mechanical properties. *J. Alloys Compd.* **2018**, *744*, 759–768. [[CrossRef](#)]
43. Sun, H.Y.; Cheng, L.; Lu, Y.L.; Ma, M.; Liu, W.C. A technique for improving deformability of the 6061Al-TiC_p composites by spark plasma sintering and hot rolling. *Mater. Lett.* **2024**, *355*, 135290. [[CrossRef](#)]
44. Olumor, I.D.; Wiśniewska, M.; Torresani, E.; Olevsky, E.A. Additive manufacturing and spark plasma sintering as effective routes for manufacturing of AISI 316L austenitic stainless steel—WC composites. *J. Mater. Res. Technol.* **2023**, *26*, 3234–3244. [[CrossRef](#)]
45. Tokita, M. Trends in Advanced SPS Spark Plasma Sintering Systems and Technology. *J. Soc. Powder Technol. Jpn.* **1993**, *30*, 790–804. [[CrossRef](#)] [[PubMed](#)]
46. Omori, M. Sintering, consolidation, reaction and crystal growth by the spark plasma system (SPS). *Mater. Sci. Eng. A* **2000**, *287*, 183–188. [[CrossRef](#)]
47. Mamedov, V. Spark plasma sintering as advanced PM sintering method. *Powder Metall.* **2002**, *45*, 322–328. [[CrossRef](#)]
48. Guillon, O.; Dargatz, B.; Kessel, T.; Schierning, G.; Rathel, J.; Herrmann, M. Field-Assisted Sintering Technology/Spark Plasma Sintering: Mechanism. *Mater. Technol. Dev.* **2014**, *16*, 830–849.
49. Smits, F.M. Measurement of Sheet Resisistivities with the Four-Point Probe. *Bell Syst. Tech. J.* **1958**, *37*, 711–718. [[CrossRef](#)]
50. Boczkal, G.; Perek-Nowak, M. Reconfiguration of point defects in FCC and HCP metals at initial stage of recovery process. *Arch. Metall. Mater.* **2014**, *59*, 1733–3490. [[CrossRef](#)]
51. Yu, P.F.; Zhang, L.J.; Cheng, H.; Zhang, H.; Ma, M.Z.; Li, Y.C.; Li, G.; Liaw, P.K.; Liu, R.P. The high-entropy alloys with high hardness and soft magnetic property prepared by mechanical alloying and high-pressure sintering. *Intermetallics* **2016**, *70*, 82–87. [[CrossRef](#)]
52. Suryanarayana, C. Mechanical alloying and milling. *Prog. Mater. Sci.* **2001**, *46*, 1–184. [[CrossRef](#)]
53. Ružić, J.; Stašić, J.; Marković, S.; Raić, K.; Božić, D. Synthesis and Characterization of Cu-ZrB₂ Alloy Produced by PM Techniques. *Sci. Sinter.* **2014**, *46*, 217–224. [[CrossRef](#)]
54. Fan, Z.; Tsakiroopoulos, P.; Miodownik, A.P. Prediction of Young’s modulus of particulate two phase composites. *Mater. Sci. Technol.* **1992**, *8*, 922–929. [[CrossRef](#)]
55. Prusa, V.; Trnka, L. Mechanical response of elastic materials with density dependent Young modulus. *Appl. Eng. Sci.* **2023**, *14*, 100126.
56. Swikker, K.R.J.; Kanagasabapathy, H.; Manickam, I.N.; Ponraj Nadar, N.V.; Alwin, S. Effect of sintering temperature on the microstructure and properties of graphite/copper matrix composite. *Nonferrous Met. Sci. Eng.* **2020**, *11*, 51–59.
57. Su, Y.; Jiang, F.; Long, M.; Wu, F.; Xiao, Z.; Wu, M. Microstructure and frictional properties of copper-tin composites containing graphite and MoS₂ by rapid hot-press sintering. *Tribol. Int.* **2023**, *183*, 108392. [[CrossRef](#)]
58. Soloviova, T.O.; Solodkyi, I.V.; Loboda, P.I. Spark Plasma Sintering of Cu-(LaB₆-TiB₂) Metal-Ceramic Composite and Its Physical-Mechanical Properties. *J. Superhard Mater.* **2019**, *41*, 213–220. [[CrossRef](#)]
59. Wei, H.; Zou, J.; Li, X.; Zhan, W.; Li, F. Friction and wear behavior of copper/graphite/Ti₂SnC composites fabricated by spark plasma sintering (SPS). *Wear* **2023**, *512–513*, 204530. [[CrossRef](#)]
60. Morz, C. Annual mineral review. Zirconium diboride. *Am. Ceram. Soc. Bull.* **1995**, *74*, 165–166.

61. Fahrenholtz, W.G.; Hilmas, G.E.; Talmy, I.G.; Zaykoski, J.A. Refractory Diborides of Zirconium and Hafnium. *J. Am. Ceram. Soc.* **2007**, *90*, 1347–1364. [[CrossRef](#)]
62. Li, M.; Zinkle, S.J. Physical and mechanical properties of copper and copper alloys. *Compr. Nucl. Mater.* **2012**, *4*, 667–690.
63. Azimi, M.; Akbari, G.H. Development of nano-structure Cu–Zr alloys by the mechanical alloying process. *J. Alloys Compd.* **2011**, *509*, 27–32. [[CrossRef](#)]
64. Robert, A. (Ed.) *Encyclopaedia of Physical Science and Technology, Reference Work*, 3rd ed.; Meyers, Ramtech, Inc.: Tarzana, CA, USA, 2001; ISBN 978-0-12-227410-7.
65. Chakrabarti, D.J.; Laughlin, D.E. The B-Cu (Boron-Copper) system. *Bull. Alloy Phase Diagr.* **1982**, *3*, 564–570. [[CrossRef](#)]

Disclaimer/Publisher’s Note: The statements, opinions and data contained in all publications are solely those of the individual author(s) and contributor(s) and not of MDPI and/or the editor(s). MDPI and/or the editor(s) disclaim responsibility for any injury to people or property resulting from any ideas, methods, instructions or products referred to in the content.